Proceeding of the IEEE
International Conference on Robotics and Biomimetics
Dali, China, December 2019

Simulation and Kinematic Modelling of a Wire-driven Active Interventional Catheter for PCI

Min Liu, Lisheng Xu, Lin Qi*
College of Medicine and Biological Information Engineering, Northeastern University, Shenyang 110819, China
*corresponding author: qilin@bmie.neu.edu.cn

***Abstract* - Because of the difficulty of traditional interventional catheter operation and limited range of motion and flexibility, we adopt a structure of an active interventional catheter-based on wire driven. A three-dimensional structural model of active interventional catheter was built in CAD software. The kinematics analysis of the catheter-based on the large deflection theory and the circular arc hypothesis. The operational active interventional catheter was simulated and analyzed based on Adams software. Simulation is based on kinematic modelling demonstrates this advantage.**

Index Terms - active interventional catheter; large deflection theory; circular arc hypothesis; kinematics modelling

I. Introduction

At present, the main treatments for cardiovascular diseases include surgical treatment, radiotherapy, drug therapy and minimally invasive interventional surgery [1]. Minimally invasive surgery is guided by X-ray equipment [2], the surgeon deal with the surgical object by operating the interventional catheter, and treats the disease by controlling the end of the interventional catheter. MIS brings a variety of benefits to patients, such as faster postoperative exercise and recovery, shorter hospital stays, lower recurrence rates and postoperative complications, and smaller wounds, more and more widespread application in the treatment of cardiovascular diseases [3]. The catheter tip of traditional interventional catheters with a shape like a blood vessel, so he can superior pass the bent portion of the blood vessel. Traditional interventional catheter has issues of destitute security, limited bending capability and poor environmental adaptability. However, the active interventional catheter robot makes up for the deficiencies in this area.

To solve these drawbacks, it is desired that the tip of the catheter be flexible and can be steered. Shape memory alloys (SMAs) active interventional catheter have been proposed, allowing for bending, extending/contracting, and torsional and stiffness control [4]. In 1991, Dario et al. [5] proposed a catheter actuated by four SMA wires (90° apart). In 1996, Lim et al. [6] designed a multi-joint and multi-directional catheter with an SMA coil actuator that can bend in any direction. In 2004, Langelaar and van Keulen [7] proposed the use of a small diameter tube of nickel-titanium alloy catheter by laser. The output displacement is large, but manufacturing process complex, structure complex, the nonlinear behavior of the strain [8, 9] and high temperature may cause the injury of cells or tissue. In 2013, Rioux et al. [10] designed an activate catheter having internal magnet actuation. Although it has been applied in clinical use, the magnetic actuation catheter system is still large-size, expensive with strict magnetic shielding requirement. In 2012, Ikuta et al. [11] designed a two-section hydraulic pressure driven active catheter. Two valves of different pressures control the hydraulic bellows. The catheter driven by hydraulic pressure is safer, but the output force is relatively small, and the catheter needs relatively complex fabricating techniques. It may have a leakage problem and large size [12]. The largest and most commercial active interventional catheter drive technology is cable-driven or tendon-driven. In 2009, Camarillo et al. [13] designed a catheter with two articulated sections and two tendons per section arranged antagonistically from the distal to proximal. Tendon-driven has simple structure, large driving force and quick response. However, cable itself has a slight elastic deformation; thus, it is difficult to achieve high precision control and to predict its deformation trajectory.

For active interventional catheters, kinematic analyzes is exceptionally vital. Fu et al. proposed a large deflection theory based on the shape memory alloy catheter to study the relationship between driving force and bending angle of the catheter [14]. Zhao et al. proposed the arc hypothesis [15]. This paper confirms the possibility and application scope of these two hypothetical on a wire-driven catheter, and focuses on the relationship between drive wire displacement and catheter bending angle by Adams simulation. Kinematic modelling and simulation show that it can accurately predict the deformation of the catheter. It suggests the potential for impact in the area of minimally invasive medical procedures.

The rest of this paper organize as follows: Section II describes the structure of catheter, section III describes the kinematics modeling of the catheter-based on the large deflection theory and the circular arc hypothesis, section IV describes the simulation of catheter, section V presents simulation results and discussions, and section VI makes the conclusion. The details of mathematical derivation are listed in the Appendix.

II. Catheter Structure

To overcome the disadvantages of the traditional interventional catheter, this paper presents a modular wire-driven unit, as shown in Fig. 1.

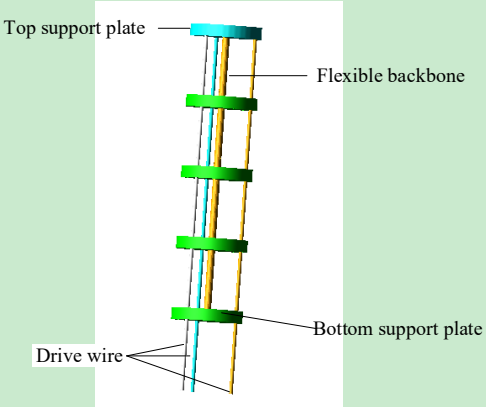

Fig. 1 Schematic of the active interventional catheter.

Advantages of modular design: select the appropriate single catheter unit diameter and length based on the shape of the target vessel prior to surgery. The structure of the catheter can achieve rapid reconfiguration based on the interventional environment. The middle flexible backbone is made of nickel-

978-1-7281-6321-5/19//$31.00 ©2019 IEEE

titanium alloy. The middle flexible backbone is connected to two adjacent support plates of the catheter. The flexible backbone supports the overall shape of the continuum robot and provides the deformation restoring force. When the catheter is bent, the flexible backbone plays a supporting role, and the axial length of the flexible backbone remains unchanged. The three wires are made of polyethylene and alternately distributed by 120 degrees on the support plate.

III. KINEMATIC ANALYSIS

For continuum active interventional catheter, it is complicated and hard to establish the direct mapping relationship between actuator space and task space. Therefore, the kinematics modelling of active interventional catheter has two parts [16] including forward kinematics and inverse kinematics, as shown in Fig. 2.

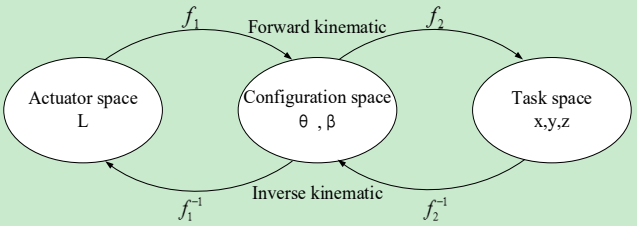

Fig. 2 The relationship among actuator space, configuration space and task space.

At present, the kinematics analysis of continuous catheter robot is mainly based on the circular arc hypothesis [15]. In this paper, we will introduce another large deflection theory [14] for kinematic analysis of active interventional catheters. In addition, we will introduce and compare these two methods as following:

A. Large Deflection Theory

In this paper, to simplify the model, three essential assumptions are made:

(1) Ignoring the effect of the weight of each component on bending and deflection.

(2) Ignoring the amount of twist of the flexible backbone during the bending process.

(3) The length of the centerline of the catheter is not changed during the bending process.

The bending of each unit and the entire catheter is in principle identical. Therefore, only one of the bending unit needs to be analyzed. A unit of the active interventional catheter that is at a bending angle of β_0 and is at the deflecting angle of θ_0 shows in Fig.3.

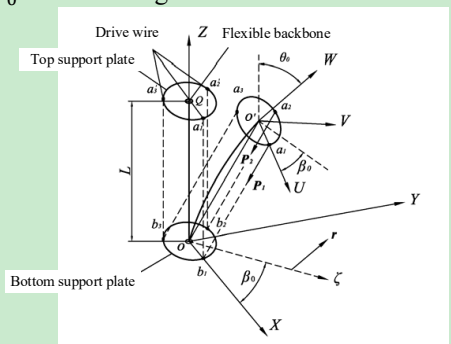

Fig. 3. Bending geometry model of a single section.

The bending and deflection of the active interventional catheter in any direction is accomplished by controlling one or two adjacent drive wires. The output loads of the driving wires are $P_i(i = 1, 2, 3)$. Bending model of the equivalent bar is shown as Fig. 4.

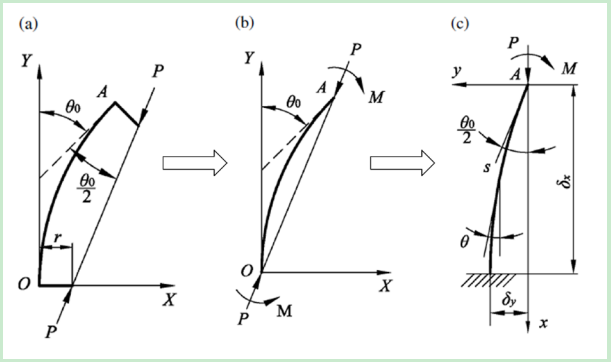

Fig. 4. Bending model of the equivalent bar [16]. (a) Equivalent bar applied by load P with eccentric displacement r. (b) Equivalent analysis of (a) in which the load P is equivalently replaced by the couple of moment M and load P with zero eccentric displacement. (c) Half model of equivalent bar

From Fig. 3 and Fig. 4 we can conclude that this is a lateral bending problem of the cantilever bar. The differential equation of the deflection curve [17] of the equivalent bar axis shown below.

$$(E \cdot I) \cdot \frac{1}{\rho} + P \cdot y + M = 0 \tag{1}$$

where ρ is the curvature radius, E is the elastic modulus of the equivalent bar, I is the moment of inertia the equivalent bar, M is combined moment acting on the equivalent bar, P is a combined force acting on the equivalent bar.

In coordinates $\sum AXY$, the expression of the half model deflection curve of the axis of the active interventional catheter is given by:

$$x + \frac{2}{k} \cdot E(\frac{\lambda}{2}, \phi) - \frac{1}{k} \cdot K(\frac{\lambda}{2}, \phi) - \delta_x = 0 \tag{2}$$

$$\varphi = \arccos(1 - \frac{(\delta_y - y) \cdot k}{\lambda}) \tag{3}$$

where $K(\frac{\lambda}{2}, \phi)$ is the incomplete elliptic integral of the first kind, $E(\frac{\lambda}{2}, \phi)$ is the incomplete elliptic integral of the second kind.

If the catheter tip has n sections, the length change of the drive wire is approximately h_{ni}.

$$h_{ni} \approx n \cdot |L - l_i| \tag{4}$$

B. Circular Arc Hypothesis

In order to simplify the model, four important assumptions are made:

(1) The length of the centerline of the catheter is not changed during the bending process.

(2) The curve shape of the centerline of the catheter is similar to that of curvature arc.

(3) Ignoring the effect of the weight of each component on bending and deflection.

(4) Ignoring the amount of twist of the flexible backbone during the bending process.

The bending model of the interventional catheter under the circular arc hypothesis is shown in Fig. 5 [15].

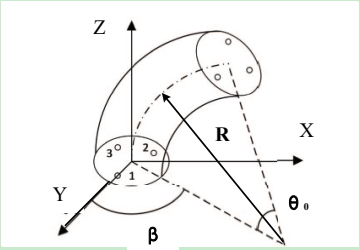

Fig. 5. Bending method based on the circular arc hypothesis.

Under the premise of known joint angles of each single catheter, the length of the drive wire is as follows:

$$l_{i1} = l - r \cdot \theta_i \cdot \cos\beta_i \tag{5}$$

$$l_{i2} = l - r \cdot \theta_i \cdot \cos(\beta_i - \frac{2\pi}{3}) \tag{6}$$

$$l_{i3} = l - r \cdot \theta_i \cdot \cos(\beta_i + \frac{2\pi}{3}) \tag{7}$$

Equation (4) illustrates the calculation of β_i.

$$\beta_i = \arccos\left(\frac{l - l_{i1}}{r \cdot \theta_i}\right) \tag{8}$$

Equation (5) illustrates the calculation of θ_i.

$$\theta_i = \arctan\frac{2(l_{i2} - l_{i3})}{l_{i2} + l_{i3} - 2l} \tag{9}$$

IV. Numerical Simulation

We performed numerical simulation based on multi-body dynamics by using Adams to observe the deformation of the active interventional catheter using a solver (Version 2017.2: Virtual Motion Inc., USA). The flexible skeleton and support plate are built in CAD software NX Nastran and SolidWorks, respectively. Finally, the support plate and flexible skeleton are imported into Adams. The drive wire is established in Adams, the drive wire is fixed with the top support plate, and contact is set between the drive wire and the middle support plate. The specific modelling and simulation process is simulation shown in Fig. 6. The dimension of active intervention catheter is shown in Fig. 7. The geometrical and physical parameters of the Adams model for active interventional catheter is in Table I.

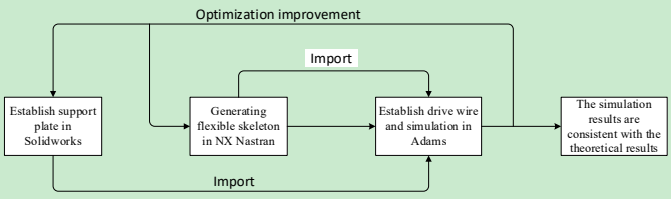

Fig 6. Modeling and simulation process.

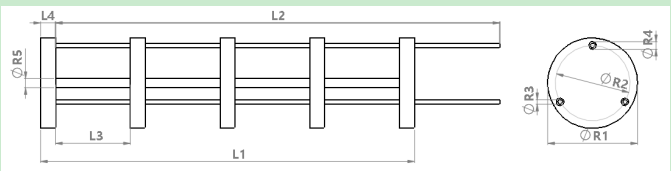

Fig 7. Schematic of active intervention catheter

Table I
GEOMETRICAL AND PHYSICAL PARAMETERS OF THE ADAMS MODEL

Variable	Value	Description
R1	6 mm	Outer diameter of the catheter
R2	5 mm	Diameter of the circle where the wire hole is located
R3	0.3mm	Diameter of the wire
R4	0.5mm	Diameter of the wire hole
R5	0.6mm	Diameter of flexible backbone
L1	25mm	Length of the catheter
L2	30mm	Length of the wire
L3	5mm	Length of flexible backbone
L4	1mm	Thickness of the support plate
E1	800Mpa	Young's Modulus of wire
E2	80Gpa	Young's Modulus of flexible backbone[18]

In the simulation, the bottom support plate was fixed and the yellow wire was pulled to bend active interventional catheter toward the right. Fig. 8 shows the active interventional catheter shape in the simulation results that bends at 0°, 5°, 15°, 30°, 45° and 60°, respectively.

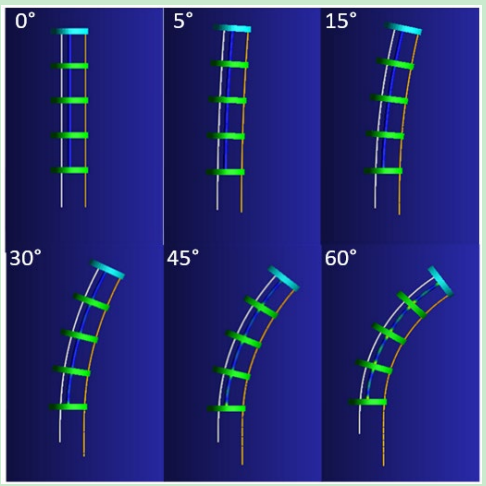

Fig. 8 The result of bending the catheter at different angles.

V. Results and Discussion

Fig. 9 shows a comparison of the simulation axis curve shape of the catheter while bending with the axis curve shapes by large deflection theory and by circular arc hypothesis.

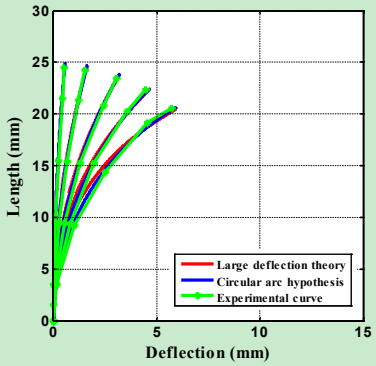

Fig 9. Schematics of deflection curve using three methods.

From Fig. 9 we can see that the calculated deflection of catheter by large deflection theory is almost entirely the same as the simulation curve and the calculated result of the axis curve by the circular arc hypothesis is very close to the curve of the simulation when the bending angle is less than 30°. When the bending angle is 30° and 60°, the calculation results from the axis curve calculated according to the large deflection

theory and the axis curve assumed by the circular arc hypothesis has a specific deviation from the fitting curve of the simulation results.

Table II shows the comparative displacement results of a wire when the catheter bends to 5°, 15°, 30°, 45° and 60° by simulation, large deflection theory and circular arc hypothesis. The results indicate that the calculated displacement of the wire by large deflection theory is very close to the simulation results; however, there is a significant deviation from the calculated results by circular arc hypothesis and the simulation results.

Table II
THE DISPLACEMENTS OF WIRE UNDER THE SAME BENDING ANGLES

Bending angle θ(°)	Simulation results (mm)	Large deflection theory(mm)	Circular arc hypothesis (mm)
5	0.243	0.283	0.218
15	0.799	0.880	0.654
30	1.693	1.667	1.308
45	2.617	2.472	1.963
60	3.695	3.281	2.610

VI. Conclusions

Through the above experiments and comparisons, we can conclude that the calculated results of the axis curve by large deflection theory have higher accuracy. When the bending angle is less than 30°, the circular arc hypothesis can also be used to predict the deformation of the catheter. When the bending angle is greater than 30°, the deflection of the catheter must be predicted by the large deflection theory.

Acknowledgment

This work was supported by the National Natural Science Foundation of China (Nos.61773110, 61374015, and 61202258), Natural Science Foundation of Liaoning Province (Key Program) (No.20170520180), and the Fundamental Research Funds for the Central Universities (Nos.N161904002, N171904009 and N172008008).

References

[1] Dogangil G, Davies B L, Baena F R Y. A review of medical robotics for minimally invasive soft tissue surgery [J]. Proceedings of the Institution of Mechanical Engineers Part H Journal of Engineering in Medicine, 2010, 224(5):653-679.
[2] Gomes P. Surgical robotics: Reviewing the past, analyzing the present, imagining the future [J]. Robotics & Computer Integrated Manufacturing, 2011, 27(2):261-266.
[3] Rosen M, Ponsky J. Minimally invasive surgery [J]. Endoscopy, 2001, 33(04): 358-366.
[4] Makishi W, Matunaga T, Haga Y, et al. Active Bending Electric Endoscope Using Shape Memory Alloy Coil Actuators [C]. IEEE/RAS-EMBS International Conference on Biomedical Robotics & Biomechatronics. 2006.
[5] Dario P, Valleggi R, Pardini M, et al. A miniature device for medical intracavitary intervention[C]//Micro Electro Mechanical Systems, Mems 91, An Investigation of Micro Structures, Sensors, Actuators, Machines & Robots IEEE. IEEE, 2002.
[6] Lim G, Park K, Sugihara M, et al. Future of active catheters [J]. Sensors & Actuators A Physical, 1996, 56(1):113-121.
[7] Langelaar M, van Keulen F. Modeling of a shape memory alloy active catheter[C]//45th AIAA/ASME/ASCE/AHS/ASC Structures, Structural Dynamics & Materials Conference. 2004: 1653.
[8] Jayender J, Azizian M, Patel R V. Autonomous Image-Guided Robot-Assisted Active Catheter Insertion [J]. IEEE Transactions on Robotics, 2008, 24(4):858---871871.
[9] Jayender J, Patel RV, Nikumb S. Robot-assisted Active Catheter Insertion: Algorithms and Experiments [J]. The International Journal of Robotics Research, 2009, 28(9):1101-1117.
[10] Rioux R, Casey T V. Magnetically steerable catheter assembly: U.S. Patent 8,394,091[P]. 2013-3-12.
[11] Ikuta K, Matsuda Y, Yajima D, et al. Pressure Pulse Drive: A Control Method for the Precise Bending of Hydraulic Active Catheters [J]. IEEE/ASME Transactions on Mechatronics, 2012, 17(5):876-883.
[12] Hu X, Chen A, Luo Y, et al. Steerable catheters for minimally invasive surgery: a review and future directions [J].
[13] Camarillo DB, Carlson CR, Salisbury JK. Configuration Tracking for Continuum Manipulators with Coupled Tendon Drive [J]. IEEE Transactions on Robotics, 2009, 25(4):798-808.
[14] Fu Y, Li X, Wang S, et al. Research on the axis shape of an active catheter [J]. International Journal of Medical Robotics & Computer Assisted Surgery, 2010, 4(1):69-76.
[15] Peng Z, Bai C, Yaoyao W, et al. Kinematic analysis of cable-driven hyper-redundant catheter robot[C]// International Conference on Mechatronics & Machine Vision in Practice. IEEE, 2017.
[16] Li Z, Chiu P W Y, Du R. Design and kinematic modeling of a concentric wire-driven mechanism targeted for minimally invasive surgery[C]// IEEE/RSJ International Conference on Intelligent Robots & Systems. IEEE, 2016.
[17] Timoshenko SP, Gere JM. Theory of Elastic Stability, 2nd ed. Science Press: Peking, 1965.
[18] Yamada A, Naka S, Nitta N, et al. A Loop-Shaped Flexible Mechanism for Robotic Needle Steering [J]. IEEE Robotics and Automation Letters, 2018, 3(2):648-655.

Appendix

The following is a detailed derivation process of the large deflection theory. From Fig. 3 and Fig. 4 we can conclude that this is a lateral bending problem of the cantilever bar. The differential equation of the deflection curve [17] of the equivalent bar axis shown below.

$$(E \cdot I)\frac{1}{\rho} + P \cdot y + M = 0 \tag{A.1}$$

where ρ is the curvature radius.

The deflection curve equation of the equivalent bar is shown below.

$$\frac{1}{\rho} = \frac{d\theta}{ds} \tag{A.2}$$

where $\theta \in [0, \frac{\theta_0}{2}]$, θ is the bending angle of the catheter.

In order to simplify the equation, we introduce a new variable k, defined as:

$$k^2 = \frac{P}{(E \cdot I)} \tag{A.3}$$

From equations (1) and (2), the large deflection curve differential equation of the equivalent bar is given by:

$$\frac{d^2\theta}{ds^2} + k^2 \cdot \sin\theta = 0 \tag{A.4}$$

To integrate equation (4) and consider the boundary conditions, we can get:

$$ds = -\frac{d\theta}{k \cdot \sqrt{4\sin^2\frac{\theta_0}{4} + k^2 \cdot (\frac{M}{P})^2 - 4\sin^2\frac{\theta}{2}}} \tag{A.5}$$

In order to simplify the equation, we introduce a new variable φ, defined as:

$$\sin\varphi = \frac{2\sin\frac{\theta}{2}}{\sqrt{4\sin^2\frac{\theta_0}{4} + k^2 \cdot (\frac{M}{P})^2}} \tag{A.6}$$

Where $\varphi \in [0, \varphi_0]$.

$$\varphi_0 = \arcsin \frac{2\sin\frac{\theta_0}{4}}{\sqrt{4\sin^2\frac{\theta_0}{4} + k^2 \cdot (\frac{M}{P})^2}} \quad (A.7)$$

In order to simplify the equation, we introduce a new variable λ, defined as:

$$\lambda = \sqrt{4\sin^2\frac{\theta_0}{4} + k^2 \cdot (\frac{M}{P})^2} \quad (A.8)$$

Moreover, we can obtain:

$$\sin\frac{\theta}{2} = \frac{\lambda}{2} \cdot \sin\varphi \quad (A.9)$$

From equation (5) and equation (9), we can obtain:

$$\frac{L}{2} = \int_s ds = -\frac{1}{k} \cdot K(\frac{\lambda}{2}, \varphi_0) \quad (A.10)$$

where L is length of the catheter.

The transfer matrix from $\sum O'UVW$ to $\sum OXYZ$ can be obtained from Fig. 3.

$$R_{r,\theta_0} = \begin{bmatrix} S^2\beta_0 \cdot (1-C\theta_0) + C_{\theta_0} & -S\beta_0 \cdot C\beta_0 \cdot (1-C\theta_0) & C\beta_0 \cdot S\theta_0 \\ -S\beta_0 \cdot C\beta_0 \cdot (1-C\theta_0) & C^2\beta_0 \cdot (1-C\theta_0) + C\theta_0 & S\beta_0 \cdot S\theta_0 \\ -C\beta_0 \cdot S\theta_0 & -S\beta_0 \cdot S\theta_0 & C\theta_0 \end{bmatrix} \quad (A.11)$$

where $C\beta_0 = cos\,\beta_0$, $S\beta_0 = sin\,\beta_0$. β is the rotation angle of the catheter.

The unit direction vector of $O'a_i(i = 1,2,3)$ in $\sum O'UVW$ is d_1', d_2' and d_3' :

$$\begin{aligned} d_1' &= (1,0,0)^T \\ d_2' &= (-\frac{1}{2}, \frac{\sqrt{3}}{2}, 0)^T - \frac{1}{2} \\ d_3' &= (-\frac{1}{2}, \frac{\sqrt{3}}{2}, 0)^T \end{aligned} \quad (A.12)$$

The unit direction vector of $O'a_i(i = 1,2,3)$ in $\sum OXYZ$ is d_i.

$$d_i = R_{r,\theta_0} \cdot d_i'(i = 1,2,3) \quad (A.13)$$

The unit direction vector of OO' in $\sum OXYZ$ is c.

$$c = (-\sin(\frac{\theta_0}{2}) \cdot \cos\beta_0, \sin(\frac{\theta_0}{2}) \cdot \sin\beta_0, -\cos(\frac{\theta_0}{2}))^T \quad (A.14)$$

$\phi_i(i = 1,2,3)$ is the angle between $O'a_i$ and OO', defined as:

$$cos\phi_i = \frac{d_i \cdot c}{|d_i| \cdot |c|} \quad (A.15)$$

According to the sine theorem:

$$M = \frac{sin\frac{\pi}{3} \cdot sin\phi_i \cdot sin\phi_j}{sin\phi_j \cdot sin(\frac{2\pi}{3}m - \beta_0) + sin\phi_i \cdot sin(\beta_0 - \frac{2\pi}{3}m + \frac{2\pi}{3})} \cdot P \cdot r \quad (A.16)$$

where r is radius of the circle where the wire hole is located. In the above formula:

$$\begin{aligned} &0 \le \beta_0 \le \frac{2\pi}{3}, i = 1, j = 2, m = 1 \\ &\frac{2\pi}{3} \le \beta_0 \le \frac{4\pi}{3}, i = 2, j = 3, m = 2 \\ &\frac{4\pi}{3} \le \beta_0 \le 2\pi, i = 3, j = 1, m = 3 \end{aligned}$$

According to the above formula, P, M and k can be obtained by using the dichotomy.

From Fig.4 (c), we can obtain:

$$dy = \sin\theta \cdot ds \quad (A.17)$$

From equations (5), equation (9) and (15), the maximal deflection of y orientation is solved as:

$$\delta_y = \frac{\lambda}{k} \cdot \int_0^{\phi_0} sin\phi d\phi = \frac{\lambda}{k} \cdot (1 - cos\phi_0) \quad (A.18)$$

Using the same method, we can obtain:

$$\delta_x = \frac{2}{k} \cdot \int_0^{\phi_0} \sqrt{1 - \frac{\lambda^2}{4}\sin^2\phi} d\phi - \int_s ds = \frac{2}{k} \cdot E(\frac{\lambda}{2}, \phi_0) - \frac{L}{2} \quad (A.19)$$

$E(\lambda/2, \phi_0)$ is an incomplete elliptic integral of the second kind.

Coordinates of joint 2 in $\sum OXYZ$ is:

$$(X_{o'}, Y_{o'}, Z_{o'}) = (2\delta_x \cdot \sin\frac{\theta_0}{2} \cdot \cos\beta_0, 2\delta_x \cdot \sin\frac{\theta_0}{2} \cdot \sin\beta_0, 2\delta_x \cdot \cos\frac{\theta_0}{2}) \quad (A.20)$$

Then, in coordinates $\sum AXY$, the expression of the half model deflection curve of the axis of the active interventional catheter is given by:

$$x + \frac{2}{k} \cdot E(\frac{\lambda}{2}, \phi) - \frac{1}{k} \cdot K(\frac{\lambda}{2}, \phi) - \delta_x = 0 \quad (A.21)$$

$$\varphi = \arccos(1 - \frac{(\delta_y - y) \cdot k}{\lambda}) \quad (A.22)$$

where $0 \le x \le \delta_x$.

Solving the length of each drive wire in the predicted attitude is a kinematic inverse problem. The homogeneous transformation matrix from $\sum OXYZ$ to $\sum O'UVW$ is as follows:

$$T = Rot(r, \theta_0) \cdot Trans(X_{o'}, Y_{o'}, Z_{o'}) \quad (A.23)$$

In the formula:

$$Trans(X_{o'}, Y_{o'}, Z_{o'}) = \begin{bmatrix} 1 & 0 & 0 & X_{o'} \\ 0 & 1 & 0 & Y_{o'} \\ 0 & 0 & 1 & Z_{o'} \\ 0 & 0 & 0 & 1 \end{bmatrix} \quad (A.24)$$

$$Rot(r, \theta_0) = \begin{bmatrix} R_{r,\theta_0} & 0 \\ 0 & 1 \end{bmatrix} \quad (A.25)$$

We can get the coordinates of $a_i(i = 1,2,3)$ in $\sum O'UVW$ in $\sum OXYZ$.

$$P_{\sum_o} = T \cdot P_{\sum_{o'}} \quad (A.26)$$

The specific expression in the above formula is as follows:

$$P_{\sum_{o'}} = [U_{ai}, V_{ai}, W_{ai}, 1](i = 1,2,3) \quad (A.27)$$

$$(U_{ai}, V_{ai}, W_{ai}) = R \cdot d_i \quad (A.28)$$

$$P_{\sum_o} = [X_{ai}, Y_{ai}, Z_{ai}](i = 1,2,3) \quad (A.29)$$

Thus, the length of each drive wire can be obtained.

$$l_i = \sqrt{(X_{a_i} - X_{b_i})^2 + (Y_{a_i} - Y_{b_i})^2 + (Z_{a_i} - Z_{b_i})^2} \quad (A.30)$$

$(X_{bi}, Y_{bi}, Z_{bi})(i = 1,2,3)$ is the coordinate system of $b_i(i = 1,2,3)$ in $\sum OXYZ$.

$$(X_{b_i}, Y_{b_i}, Z_{b_i}) = R \cdot d_i \quad (A.31)$$

We define h_i as the amount of change in the length of the

drive wire.

$$h_i = \left| L - l_i \right| \tag{A.32}$$

If it is n-section catheter, the length change of the drive wire is approximately h_{ni}.

$$h_{ni} \approx n \cdot \left| L - l_i \right| \tag{A.33}$$